Available online at www.sciencedirect.com
SCIENCE DIRECT®
Polymer 44 (2003) 4003–4009
polymer
www.elsevier.com/locate/polymer

Effect of thermal history on free volume and transport properties of high molar mass polyethylene

B. Neway, M.S. Hedenqvist, U.W. Gedde*

Department of Fibre- and Polymer-Technology, Royal Institute of Technology, SE-100 44 Stockholm, Sweden

Received 15 October 2002; received in revised form 26 January 2003; accepted 17 February 2003

Abstract

The desorption of *n*-hexane from high molar mass polyethylene at 298 K has been studied. The polymer was given different thermal treatments to obtain differences in crystallinity, morphology and composition of the non-crystalline fraction. Crystal contents determined by Raman spectroscopy were always lower than those determined by density measurements. The systems with high crystallinity showed in relative terms a low content of interfacial component. The *n*-hexane solubilities of the samples were strictly proportional to the volume fraction of penetrable polymer (liquid-like and interfacial components) and the solubility was low in comparison with that of branched polyethylene of the same crystallinity. The Cohen–Turnbull–Fujita free volume theory was numerically capable of describing the desorption process in the polyethylenes studied. One of the methods used assumed that all three non-crystalline components—liquid-like, interfacial liquid-like and interfacial crystal core components—are penetrable by *n*-hexane and this method yielded data for the geometrical impedance factor and the fractional free volume with physically realistic trends, but the changes in the geometrical impedance factor was not in quantitative agreement with the Fricke model applied to the morphological data. This lack of numerical agreement is tentatively due to the fact that the assessment of crystal shape by transmission electron microscopy of stained sections systematically underestimates the crystal widths, particularly for the low-crystallinity samples with curved and 'twisting' crystal lamellae.

Keywords: Diffusion; Polyethylene; Free volume

1. Introduction

Diffusion in semicrystalline polymers such as polyethylene is complicated by the presence of crystallites. The crystallites in polyethylene are inpenetrable for non-reactive molecules except for the smallest gas molecules such as helium [1]. The restriction of the diffusion of the penetrant molecules to the non-crystalline phase extends the diffusion path because all the crystals along the path have to be circumvented [3,4]. The effect of the detour on the diffusivity is often quantified by the geometrical impedance factor (τ), which is defined as the ratio of the diffusivity of a hypothetical fully amorphous polymer to that of the semicrystalline polymer [4]. The geometrical impedance factor is thus always greater than unity. Both the crystallinity and the shape of the individual crystallites affect τ. The classical Fricke model [5] and more 'modern' approaches such as that of Hadgett et al. [6] using Monte Carlo simulation can be used to relate τ to the morphology. The second effect of the crystallites is that, if the amorphous chain segments have both ends anchored in one or two crystallites then the positional and conformational freedom of such piece of a chain will be reduced compared with that of a fully amorphous analogue. One possible approach to quantify the constraining effect of the crystals is to use free volume theory [7,8].

Free volume theory according to Cohen and Turnbull [9,10] and Fujita [11], hereafter referred to as the CTF model, accurately describes the desorption of hydrocarbons from polyethylene [7,8,12–14]. The following equation, shown here to present the basic concepts, provides an excellent numerical fit to experimental data:

$$D = A \exp(-(B_d/f_2)) \times \exp((B_d \nu_1^a (f_1 - f_2))/(f_2(f_2 + \nu_1^a (f_1 - f_2)))) \quad (1)$$

where D is the penetrant diffusivity, A is a factor that is

* Corresponding author. Tel.: +46-8-7907-640; fax: +46-8-208856.
E-mail address: gedde@polymer.kth.se (U.W. Gedde).

0032-3861/03/$ - see front matter © 2003 Elsevier Science Ltd. All rights reserved.
doi:10.1016/S0032-3861(03)00168-X

inversely proportional to the geometrical impedance factor, B_d is a constant that depends only on the size and shape of the penetrant molecule [13,14], ν_1^a is the penetrant concentration in the penetrable phase, f_1 is the fractional free volume of the penetrant and f_2 is the fractional free volume of the penetrable fraction of the polymer. Eq. (1) assumes that the fractional free volume of the penetrable phase is the sum of contributions from polymer and penetrant, i.e. that the volume is invariant during mixing. This assumption is valid for polyethylene and *n*-hexane [7]. The geometrical impedance factor and the fractional free volume of the penetrable fraction of the polymer are separated into different factors in Eq. (1). The product of the first two factors is the zero-concentration diffusivity. The third factor describes the concentration dependence of the diffusivity. Let us examine Eq. (1). The difficulty in defining absolute values of the fractional free volume is obvious in the literature. Values reported for the fractional free volume at the glass transition temperature can be divided into three categories: (1) ~0.02–0.03 according to Doolittle [15], Williams et al. [16] and Cohen and Turnbull [9]; (2) ~0.08 according to Simha and Somcynsky [17], Hirai and Eyring [18], and Dlubek et al. [19]; (3) ~0.3–0.4, 'van der Waals type' according to Simha and Carri [20]. Only the first type can be used to fit the experimental desorption data for polyethylene and *n*-hexane. The correct concentration dependence of the diffusivity is preserved only if $\partial f_2/\partial f_1 \approx 0.1$. If f_2 is increased by 0.05 (category $1 \Rightarrow$ category 2), then f_1 is increased by 0.50, reaching a clearly physically unrealistic value. Hence, only fractional free volume values on the scale of Doolittle, WLF and Cohen and Turnbull can give physically feasible results. In previous papers [7,8] and in the present paper, the fractional free volume value (f_1) used for *n*-hexane was, according to Fleischer [14], $f_1 = 0.168$, which yields fractional free volumes for amorphous polyethylene consistent with a fractional free volume of 0.025 at the glass transition temperature.

Previous papers [7,8] dealing with the desorption of *n*-hexane from a collection of different polyethylenes showed that the fractional free volume of the penetrable phase was strongly dependent on its total volume fraction, suggesting the presence of an interfacial penetrable component with low fractional free volume. The data obtained suggest that mass transport occurs from the liquid-like component to the interfacial component and that the penetrant molecules are trapped at the interfacial sites [8]. A problem was experienced with the heterogeneous branched polyethylenes, which showed a decrease in the geometrical impedance factor with increasing crystallinity [8]. This unusual behaviour was explained by the presence of a few extraordinarily wide crystal lamellae in the heterogeneous low crystallinity samples [8]. In the present work, high molar mass linear polyethylene has been given different thermal treatments to produce a series of samples with different degrees of crystallinity that partly covers the crystallinity range of the heterogeneous branched polyethylenes previously studied. The morphologies obtained are supposedly more uniform than in the case of the heterogeneous branched polyethylenes but the variations between the different samples are still significant. The aim of the study is to see whether the CTF model is applicable, in view of the observed trends in the lamellar structure as revealed by transmission electron microscopy.

2. Experimental

High molar mass linear polyethylene with $\bar{M}_w = 1\,040\,000$ g mol^{-1} and $\bar{M}_w/\bar{M}_n = 54.45$ was compression moulded into $30 \times 40 \times 0.70 \pm 0.13$ mm sheets in a Schwabenthan Polystat 400 s compression-moulding machine at 473 K for 10 min and then given one of the following thermal treatments: (a) quenched in an ice–water–salt mixture (sample Q); (b) cooled in air (sample A); (c) cooled at a rate of 0.2 K min^{-1} to room temperature while the pressure was maintained (sample S); (d) transferred to 401.2 ± 1 K oven chamber and kept at this temperature for 3 weeks in nitrogen, and then cooled in air to 298 K (sample IC).

Melting endotherms were obtained by heating 5 ± 0.5 mg samples at a rate of 10 K min^{-1} using a temperature- and energy-calibrated Mettler–Toledo DSC 820 with nitrogen as purge gas. Mass crystallinities ($w_{c,\rho}$) were obtained from density data at 298 K by comparing the weights of the samples in air and ethanol ($\rho = 790$ kg m^{-3}) and by then considering the densities of crystalline (1000 kg m^{-3}) and amorphous (855 kg m^{-3}) components reported by Wunderlich [21]. A top-loaded Mettler AE 100 balance with resolution 10^{-5} g and a Mettler-density determination kit ME-33360 were used. Raman spectra were recorded at 298 K in a Perkin–Elmer Spectra 2000 NIR-Raman instrument in order to determine the mass fractions of liquid-like, interfacial liquid-like, interfacial crystal core and crystal core components of the samples [22]. Each spectrum was based on 200 scans. The lamellar structure was revealed by transmission electron microscopy using a Philips Tecnai 10 electron microscope. Chlorosulphonated 50 nm sections stained with uranyl acetate according to Kanig [23] were studied in the electron microscope.

The sheets were first immersed in liquid *n*-hexane (purity 99%; Merck; density $\rho_L = 656$ kg m^{-3} at 298 K) at 298 K until sorption equilibrium was attained. The saturated sheets were then held in air at 298 K and the desorption kinetics were followed by weighing the samples on a Mettler AE balance after different periods of time until constant mass was attained.

3. Analysis of desorption data

The details regarding the numerical analysis of the desorption data have been presented before [7,8,24]. A brief description of the methods used is presented here. The thermodynamic diffusivity (D_T) is related to the fractional free volume of the penetrable phases of the polymer (f_2) according to Eq. (1). The thermodynamic diffusivity is related to the diffusivity of penetrant with the polymer as a fixed frame (D_{12}) according to [8]:

$$D_T = \frac{D_{12}}{(1-\nu_1)[(1-\nu_1^a)(1-2\chi_{12}\nu_1^a)]} \quad (2)$$

where ν_1 is the volume fraction of penetrant dissolved in the polymer, ν_1^a is the volume fraction of penetrant in the penetrable fraction of the polymer and χ_{12} is the Flory–Huggins interaction parameter. The following penetrant-concentration-dependence of χ_{12} for the binary system reported by Rogers et al. [25] was used in the analysis:

$$\chi_{12} = 0.6(1-\nu_1^a)^{-5/3} + 0.08 \quad (\text{for } \nu_1^a < 0.183) \quad (3)$$

$$\chi_{12} = 0.92 \quad (\text{for } \nu_1^a \geq 0.183)$$

Eqs. (2) and (3) were combined with Fick's second law of diffusion to yield the following differential equation:

$$\frac{\partial \nu_1}{\partial t} = \frac{\partial}{\partial x}\left[D_T(1-\nu_1^a)(1-2\chi_{12}\nu_1^a)\frac{\partial \nu_1}{\partial x}\right] \quad (4)$$

In the numerical solution, only half the plate thickness was considered. The inner boundary co-ordinate was described as an isolated point:

$$\left(\frac{\partial \nu_1}{\partial x}\right)_{x=L} = 0 \quad (5)$$

where x is the distance from the outer wall and L is half the plate thickness. During desorption, evaporation took place at the surface of the plate, and the outer boundary condition was given by:

$$D_T(1-\nu_1^a)(1-2\chi_{12}\nu_1^a)\left(\frac{\partial \nu_1}{\partial x}\right)_{x=0} = F_0(\nu_1)_{x=0} \quad (6)$$

where the rate of evaporation (F_0) was calculated from data for the initial rate of desorption according to a method proposed by Bakhouya et al. [26] to $2.51-5.45\times10^{-5}$ cm s^{-1}. Two different approaches were used: Method I: liquid-like (L), interfacial liquid-like (IL) and interfacial crystal core (ICC) components were assumed to be penetrable. Method II: L and IL components were assumed to be penetrable. In the numerical analysis of Eqs. (1)–(6), two parameters were treated as adjustable: A and f_2. Eq. (1) is based on the model of Fujita [11], who stated that the coefficient B_d for a given polymer is proportional to the size of the penetrant molecule and also dependent on the shape of the penetrant molecule. It has been reported that B_d is independent of temperature for *n*-hexane–polyethylene [13] and benzene–polyethylene [12]. These findings show that B_d remains constant independent of changes in the structure of the penetrable polymer fraction accompanying a change of temperature. Accordingly, the parameter B_d was set to 0.8 [14]. The fractional free volume of the penetrant (f_1) was set to 0.168 [14].

4. Results and discussion

4.1. Crystallinity, phase composition and morphology

Table 1 presents the crystallinities and the mass fractions obtained by Raman spectroscopy. Mass crystallinities obtained from density data ($w_{c,\rho}$) were larger than the mass fraction of crystal core component (w_{CC}) obtained by Raman spectroscopy; the average difference between the two series of data was 0.095 which was 15% of the crystal content as assessed by density measurements. This difference, $w_{c,\rho} - w_{CC}$, is significantly larger for these high molar mass linear polyethylenes than for linear polyethylenes with lower molar mass; the difference for the whole group was only 0.055 [7]. The relative mass proportions of the interfacial components to that of the liquid-like component were between 0.86 and 1.25 with the highest value for the highly crystalline IC sample. These data are consonant with the trend in earlier reported data on linear polyethylene [7,8]. The mass fraction of the interfacial component ($w_{ICC} + w_{IL}$) increased with decreasing crystallisation temperature: sample Q (low crystallisation temperature) had 28 wt% interfacial component whereas sample IC (most of the crystals were formed at 401.2 K) had only 16% interfacial component. The data were generally in accordance with the NMR data of Cheng et al. [27] for linear polyethylene: They reported mass fractions of the interfacial component of the order of 20% and, furthermore, a similar crystallisation-temperature-dependence of the mass fraction of the interfacial component as was found in the present study. It is also interesting to assess the proportion of interfacial component in the penetrable phases, ICC + IL + L or IL + L depending on the model chosen (Table 1): $(w_{ICC} + w_{IL})/(w_{ICC} + w_{IL} + w_L)$ ranged between 0.49 (sample Q) and 0.55 (sample IC); $w_{IL}/(w_{IL} + w_L)$ ranged from 0.32 (sample Q) to 0.405 (sample IC).

Table 1
Mass crystallinities and mass fractions of components by Raman spectroscopy at 298 K

Sample code	$w_{c,\rho}$ [a]	w_{CC} [b]	w_{ICC} [b]	w_{IL} [b]	w_L [b]
Q	0.536	0.426	0.144	0.137	0.293
A	0.563	0.501	0.101	0.130	0.268
S	0.630	0.558	0.096	0.114	0.234
IC	0.818	0.683	0.080	0.096	0.141

[a] From density data (s.d. ± 0.025).
[b] From Raman spectra according to Refs. [8,22]: CC = crystal core; ICC = interfacial crystal core; IL = interfacial liquid-like; L = liquid-like (s.d. ± 0.020).

The average density of the two interfacial components (ICC and IL), ρ_{ICC+IL}, at 298 K was calculated from the density data (not explicitly shown) and the Raman data presented in Table 1:

$$\rho_{ICC+IL} = \frac{w_{ICC+IL}}{1/\rho_2 - w_L/\rho_L - w_{CC}/\rho_{CC}} \quad (7)$$

where ρ_2 is the density of the sample, ρ_L is the density of the liquid-like component, which is equal to 855 kg m^{-3} [21]. The obtained vale for ρ_{ICC+IL} based on the four samples was 914 kg m^{-3}, which is in the same range as 907 kg m^{-3} obtained for a wide range of linear and branched polyethylenes [8]. The individual samples showed a standard deviation of 20–30 kg m^{-3} in ρ_{ICC+IL}.

The melting traces of samples Q, A and S were unimodal with recorded melting peak temperatures of 408.6, 410 and 413 K, respectively. Unimodal melting was expected since these samples had crystallised during steady cooling. Sample IC crystallised first under isothermal conditions (401.2 K) and then at a later stage during steady cooling to give a sample with two melting peaks; the high temperature peak constituted almost 80% of the total enthalpy of melting and was due to the melting of crystals formed during the isothermal period. The low temperature peak that appeared at 370 K is associated with the crystals formed during the cooling period.

The morphology of the samples was revealed by transmission electron microscopy of chlorosulphonic-acid-stained sections (Figs. 1(a) and (b)). The IC sample, with most of its crystals formed at high temperature (401.2 K), showed dominantly straight, thick and wide crystal lamellae (Fig. 1(a)). Crystallisation at 401.2 K is very slow and time is required to disentangle the molecules and allow the formation of well-developed crystal lamellae. Fig. 1(b) shows that the rapidly cooled sample (Q) displayed thinner, more narrow and curved crystal lamellae. The aspect ratios [width (w)/crystal thickness (L_C)] of the crystals were assessed from a series (10) of electron micrographs of each sample. The width was determined by recording the length of clearly revealed crystals. The width of a given crystal can be greater than the determined value because it is possible that the crystal 'twists', i.e. becomes tilted with respect to the electron beam outside the field within which it shows a clear contrast. Data for the crystal thickness and crystal aspect ratio (w/L_C) of the four samples studied are presented in Table 2. Both crystal thickness and crystal aspect ratio showed a pronounced increase with increasing crystallisation temperature. The change in these parameters was moderate for samples Q, A and S, whereas sample IC showed markedly thicker crystals with higher aspect ratios. Fig. 2 shows the distribution of the crystal aspect ratio for the different samples. The crystal aspect ratio distributions of samples Q, A and S were relatively similar. Sample IC showed a wider distribution in crystal aspect ratio and particularly a fraction of crystals with very high aspect ratios. The broad distribution of the aspect ratio is probably

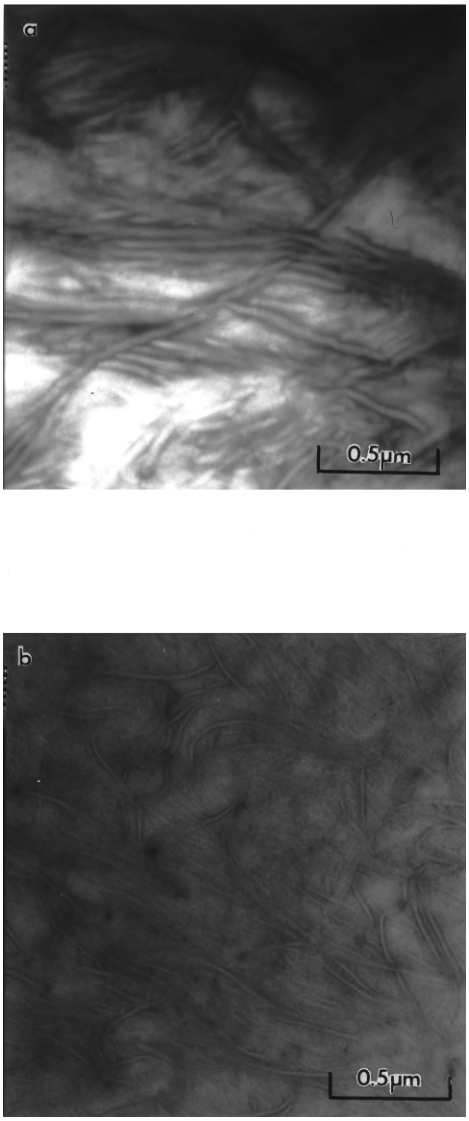

Fig. 1. Transmission electron micrographs of chlorosulphonated sections of (a) sample IC and (b) sample Q.

due to the fact that only 80% of the crystals were formed at 401.2 K whereas, the other crystals (20%) were formed during the cooling period at considerably lower temperatures.

The geometrical impedance factor (τ) was calculated according to the Fricke model [5] with the modification

Table 2
Lamella shape and calculated geometrical impedance factor

Sample code	L_C (nm)[a]	w/L_C[a]	τ[b]
Q	12.9 ± 2.1	25.7 ± 10.6	3.1 ± 0.9
A	13.9 ± 2.3	26.2 ± 11.2	3.5 ± 1.1
S	15.9 ± 2.9	31.7 ± 11.2	4.4 ± 1.3
IC	23.0 ± 4.8	49.4 ± 30.6	7.8 ± 2.9

[a] Average ± standard deviation.
[b] Geometrical impedance factor calculated from Eq. (8) also using volume crystallinity data presnted in Table 1.

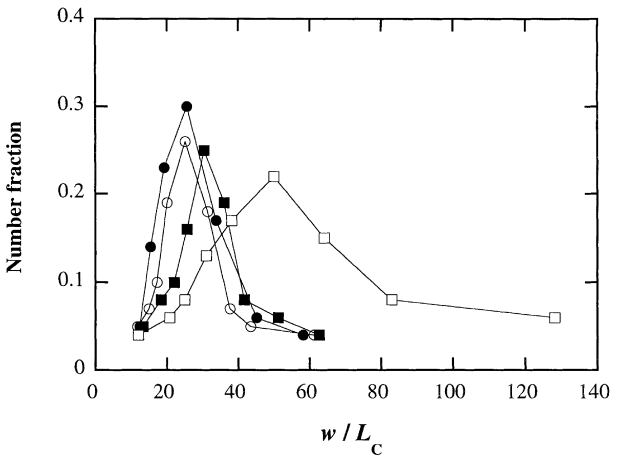

Fig. 2. Distribution of crystal aspect ratio (w/L_C) for the following samples: (●) Q; (○) A; (■) S; (□) IC.

suggested by Michaels and Bixler [2] using data for the volume crystallinity (ν_{CC}) and crystal aspect ratio (w/L_C):

$$\tau = 1 + \frac{\nu_{CC}(0.384+x^2)}{1.848-3x^2} \quad (8)$$

$$x = 0.785 - \frac{L_C}{w}$$

Table 2 presents the calculated values of τ using Eq. (8). The geometrical impedance factor increased with increasing crystallinity, (Q < A < S < IC). These calculated values are compared with values obtained from desorption data in Section 4.3.

4.2. Solubility

The penetrant concentration in the polymer at equilibrium with liquid *n*-hexane decreased with increasing crystallinity. A more detailed analysis requires a precise knowledge of the volume fraction of the penetrable component. Fig. 3 shows the volume fraction of penetrant in the polymer (ν_1^{eq}) as a function of volume fraction of penetrable polymer component (ν_{pen}). Three different cases of penetrable components were tested: (a) liquid-like component (L); (b) liquid-like and interfacial liquid-like components (L + IL); (c) liquid-like, interfacial liquid-like and interfacial crystal core components (L + IL + ICC). The experimental data [$\nu_1^{eq} = f(\nu_{pen})$] followed a linear trend with coefficients of determination (r^2) greater than 0.984. The intercepts (ν_1^{eq} value at $\nu_{pen} = 0$) for the three cases were 0.024 ± 0.018 (L), 0.011 ± 0.017 (L + IL) and 0.008 ± 0.012 (L + IL + ICC). The upper and lower limits denote the 95% confidence limits of the linear fits. A non-zero value for the intercept at the 95% confidence level is obtained only in case of L being the only penetrable component. The data thus suggest that the liquid-like and either one or two of the interfacial components are penetrable by *n*-hexane.

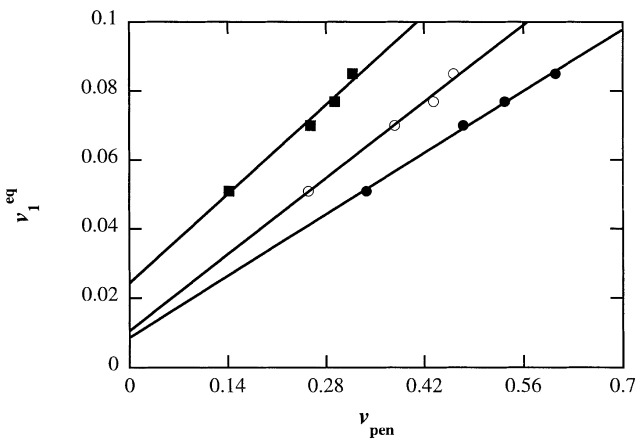

Fig. 3. Equilibrium volume fraction of *n*-hexane in polymer (ν_1^{eq}) as a function of the volume fraction of penetrable phases in dry polymer (ν_{pen}). The following assumed penetrable phases were tested: L, IL and ICC (●); L and IL (○) and L (■). The lines represent linear fits to the experimental data.

The solubilities of the studied samples were low in comparison with branched polyethylene of the same density (crystallinity). For instance, heterogeneous hexyl-branched polyethylene with a density of 937 kg m^{-3} had $\nu_1^{eq} = 0.097$ [8], whereas sample Q with a density of 927 kg m^{-3}, had $\nu_1^{eq} = 0.085$. The low solubility of the high molar mass linear polyethylenes can be attributed to their low concentration of chain ends, the lack of chain branches and the presence of chain entanglements.

4.3. Desorption data; fitting of the free volume equation

The CTF free volume theory using the starting and boundary conditions described in Section 3 and allowing two of the parameters (A and f_2) to be adjustable described the experimental desorption data exceedingly well (Sample Q; Fig. 4). The fits to the experimental desorption data of the other samples were almost as good as for sample Q. Table 3

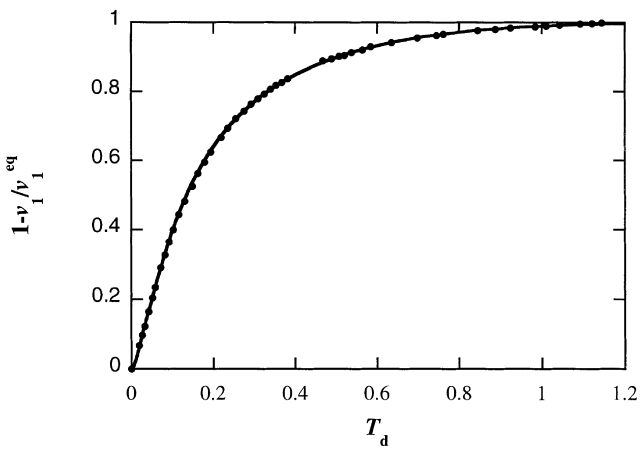

Fig. 4. Normalized *n*-hexane desorption curves for sample Q showing experimental data (points) and fitted data (line) according to method I. Dimensionless time (T_d) is defined as $T_d = \sqrt{D_{\nu_1\to 0}t/L^2}$, where $D_{\nu_1\to 0}$ is the diffusivity at $\nu_1 = 0$, t is time and L is half the specimen thickness. The *n*-hexane concentration (ν_1) is normalized with respect to the equilibrium penetrant concentration (ν_1^{eq}).

Table 3
Free volume parameters obtained by fitting according to methods I and II

Sample	Method I				Method II			
	f_2[a]	A[b,c]	$D_{\nu_1\to 0}$[d,e]	SSD[f]	f_2[g]	A[b,h]	$D_{\nu_1\to 0}$[d,i]	SSD[f]
Q	0.0436	0.5446	5.85	0.0003	0.0471	0.1302	5.57	0.0004
A	0.0424	0.5409	3.44	0.0015	0.0447	0.1860	3.22	0.0021
S	0.0421	0.5299	2.96	0.0013	0.0446	0.1667	2.70	0.0016
IC	0.0412	0.4318	1.58	0.0014	0.0445	0.0942	1.45	0.0023

[a] Relative error ±1%.
[b] In $cm^2\ s^{-1}$.
[c] Relative error ±25%.
[d] Diffusivity at $\nu_1 = 0$ in $10^{-9}\ cm^2\ s^{-1}$.
[e] Relative error ±3%.
[f] SSD = SSD between normalized experimental and fitted desorption data.
[g] Relative error ±2%.
[h] Relative error ±40%.
[i] Relative error ±5%.

presents a summary of the values obtained for the adjustable parameters (A and f_2) and the sum of squares difference (SSD) between the fitted and experimental data for the two methods employed. Method I assumed that L, IL and ICC were penetrable by *n*-hexane whereas, Method II assumed only L and ILL to be penetrable in the calculations. The SSD data displayed in Table 3 show that the goodness of fit values for both methods were relatively similar. Error analysis based on sensitivity analysis around the optimum set of the adjustable parameter values, f_2 and A, estimated by the numerical search indicated that the search was most sensitive to the parameter f_2 and the error associated with estimating A is an order of magnitude higher than the error in estimating f_2. The experimental relative error (±3–5%) arising from the determination by Raman spectroscopy of the mass fraction of the components was used in the sensitivity analysis. For method I, it was found that the relative uncertainties in f_2 and A are ±1 and ±25%, respectively. $D_{\nu\to 0}$ was estimated to be within about ±3% of the optimum values. The corresponding values for method II were ±40, ±2 and 5%.

It is interesting to examine the A and f_2 values obtained by the two methods. The pre-exponential factor (A) is inversely proportional to the geometrical impedance factor (τ). The latter was calculated by applying the Fricke model to density and transmission electron microscopy data (see Eq. (8) in Section 4.1 and Table 2). It is interesting to compare the data obtained for the pre-exponential factor using methods I and II with the theoretical values of $\tau \propto 1/A$ (Fig. 5). Method II yielded A values that showed a maximum at intermediate $1/\tau$ values (Fig. 5). In view of the large difference in morphology displayed between the different samples in Tables 1 and 2, the presence of an intermediate maximum suggests that method II is not giving physically realistic A data. Method I yielded A data that were essentially proportional to the theoretical $1/\tau(\propto A)$. However, the change in A was only a third of the change predicted by the Fricke model. The sizeable uncertainty (±25%) in the determination of A does not alter this conclusion, i.e. the relative change in A is smaller than predicted by the Fricke model based on the transmission electron microscopy data. The lack of quantitative correlation between the A data obtained by the CTF model and the Fricke model may well be due to problems in assessing the true geometry of the crystals. Only a small volume fraction of the sample is assessed and, furthermore, it is not possible to determine the exact widths of the crystals because the contrast is lost when the crystals are twisting. This means that a sample with curved and twisting lamellae will show a larger discrepancy between assessed and true crystal widths. The samples that crystallised at the lower temperatures (Q and A) showed curved lamellae with a large anticipated difference between measured and true crystal widths (Fig. 1(a)). The sample crystallised at 401.2 K showed straight crystal lamellae with a smaller expected difference between measured and true crystal

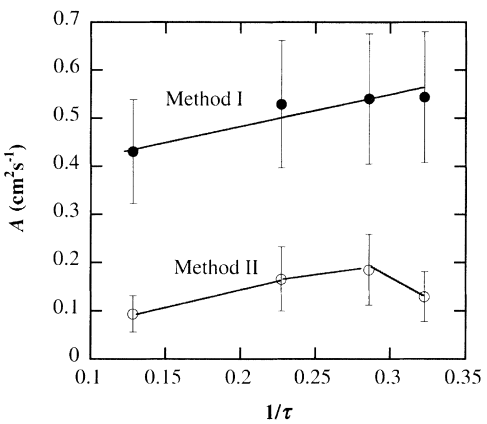

Fig. 5. The pre-exponential factor A as a function of the reciprocal of the geometrical impedance factor (τ); the latter is calculated from the crystallinity and crystal shape data presented in Tables 1 and 2 using the Fricke model [Eq. (8)]. The different results obtained by Methods I and II are displayed. The error bars indicate the uncertainty in determined A value based on the maximum error in the determination of volume fraction of penetrable polymer fraction.

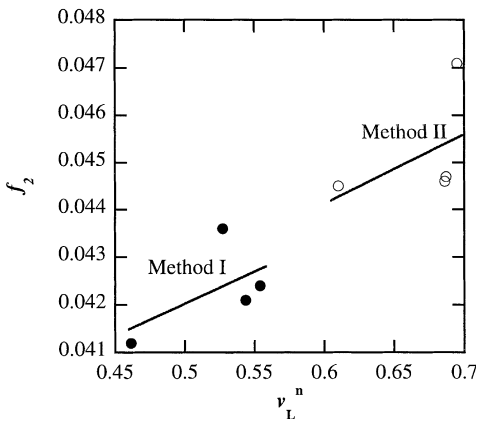

Fig. 6. The fractional free volume of penetrable polymer (f_2) as a function of the volume fraction of liquid-like component in the penetrable fraction of the polymer (ν_L^n). Note that the penetrable components are L, IL and ICC in Method I and L and IL in Method II.

widths (Fig. 1(b)). The true range in crystal aspect ratio is thus likely to be smaller than the assessed range from 25.7 to 49.4 (Table 2), which in turn would decrease the relative changes in τ and bring the theoretical and experimental data closer together. It is interesting to note that the pre-exponential factor was in accordance with the Fricke model applied to transmission electron microscopy data for a series of linear polyethylenes covering a wide crystallinity range, 0.55–0.90 [7].

It should be noted that the error in f_2 from the uncertainty in the assessment of the volume fraction of penetrable component is small (1–2%) and that the trends in the free volume data are statistically significant. The fractional free volume (f_2) obtained by method I was on average 0.0029 lower than that obtained by method II. This value is significant in view of the average difference (0.0007) obtained for a series of heterogeneous poly(ethylene-*co*-octene) samples [8]. In a previous paper [8], it was shown that f_2 was related to the volume fraction of liquid-like component in the penetrable polymer fraction, ν_L^a. The present study involved samples within a relatively narrow ν_L^a range: 0.46–0.56 (Method I) and 0.61–0.69 (Method II). The f_2 data obtained are in the same range as those reported for linear polyethylenes of lower molar masses [7]. Method I yielded f_2 values that increased in a linear fashion with ν_L^a (Fig. 6). Method II gave almost the same f_2 value for the three samples with the highest degree of crystallinity (A, S and IC). Hence, only method I gave physically realistic results.

In conclusion, the CTF theory is numerically capable of describing desorption from the high molar mass linear polyethylene studied. One of the methods used ('Method 1') assumed that all three non-crystalline components—L, ILL and ICC—are penetrable by *n*-hexane and this method yielded data for the geometrical impedance factor and fractional free volume with physically realistic trends, but the changes in the geometrical impedance factor were not in quantitative agreement with the Fricke model applied to the morphological data. It is tentatively suggested that the lack of numerical agreement is because the analysis of crystal shape by transmission electron microscopy of stained sections systematically underestimates the crystal width particularly for the low-crystallinity samples with curved and twisting crystal lamellae.

Acknowledgements

This work was sponsored by Swedish Agency for Research Co-operation with Developing Countries (SAREC/SIDA) through the joint collaboration of the University of Asmara, Eritrea and the International Science Programs (ISP) of Uppsala University, Sweden.

References

[1] Veith WR. Diffusion in and through polymers. Munich: Hanser; 1991.
[2] Michaels A, Bixler HJ. J Polym Sci 1961;50:413.
[3] Peterlin A. J Macromol Sci Phys (B) 1975;11:57.
[4] Hedenqvist M, Gedde UW. Prog Polym Sci 1996;21:299.
[5] Fricke H. Phys Rev 1924;24:575.
[6] Hadgett PM, Goldbeck-Wood G, Windle AH. Polymer 2000;41:6151.
[7] Hedenqvist M, Angelstok AA, Edsberg L, Larsson PT, Gedde UW. Polymer 1996;37:2887.
[8] Neway B, Hedenqvist MS, Mathot VBF, Gedde UW. Polymer 2001; 42:5307.
[9] Cohen MH, Turnbull D. J Chem Phys 1959;31:1164.
[10] Turnbull D, Cohen MH. J Chem Phys 1970;52:3038.
[11] Fujita H. Fortschr Hochpolym Forsch 1961;3:1.
[12] Fels M, Huang RYM. J Appl Polym Sci 1970;14:523.
[13] Kulkarni SS, Stern SA. J Polym Sci, Polym Phys 1983;21:441.
[14] Fleischer G. Colloid Polym Sci 1984;262:919.
[15] Doolittle AK. J Appl Phys 1951;22:1471.
[16] Williams ML, Landel RF, Ferry JD. J Am Chem Soc 1955;77:3701.
[17] Simha R, Somcynsky T. Macromolecules 1969;2:342.
[18] Hirai N, Eyring H. J Polym Sci 1959;37:51.
[19] Dlubek G, Stejny J, Alam MA. Macromolecules 1998;31:4574.
[20] Simha R, Carri G. J Polym Sci, Polym Phys 1994;32:2645.
[21] Wunderlich B. Crystal structure, morphology, defects. Macromolecules physics, vol. 1. New York: Academic Press; 1973.
[22] Mutter R, Stille W, Strobl G. J Polym Sci, Polym Phys 1993;31:99.
[23] Kanig G. Colloid Polym Sci 1977;255:1005.
[24] Hedenqvist MS, Gedde UW. Polymer 1999;40:2381.
[25] Rogers CE, Stannett V, Szwarc M. J Phys Chem 1959;63:1406.
[26] Bakhouya A, Brouzi AE, Bouzon J, Vergnaud JM. Plast Rubber Compos Process Appl 1993;19:77.
[27] Cheng J, Fone M, Reddy VN, Schwartz KB, Fisher HP, Wunderlich B. J Polym Sci, Polym Phys 1994;32:2683.